A stabilized MITC finite element for accurate wave response in Reissner–Mindlin plates

Lonny L. Thompson *, Sri Ramkumar Thangavelu

Department of Mechanical Engineering, Clemson University, Clemson, SC 29634, USA

Abstract

Residual based finite element methods are developed for accurate time-harmonic wave response of the Reissner–Mindlin plate model. The methods are obtained by appending a generalized least-squares term to the mixed variational form for the finite element approximation. Through judicious selection of the design parameters inherent in the least-squares modification, this formulation provides a consistent and general framework for enhancing the wave accuracy of mixed plate elements. In this paper, the mixed interpolation technique of the well-established MITC4 element is used to develop a new mixed least-squares (MLS4) 4-node quadrilateral plate element with improved wave accuracy. Complex wave number dispersion analysis is used to design optimal mesh parameters, which for a given wave angle, match both propagating and evanescent analytical wave numbers for Reissner–Mindlin plates. Numerical results demonstrates the significantly improved accuracy of the new MLS4 plate element compared to the underlying MITC4 element.

Keywords: Finite element method; Reissner–Mindlin plate; Mixed interpolation

1. Introduction

When modeling the time-harmonic response of elastic structures, accurate plate and shell elements are needed to resolve both propagating and evanescent waves over a wide range of frequencies and scales. The propagating waves are characterized by sinusoidal components with phase speed determined by the material properties and thickness of the plate, while the evanescent waves are characterized by exponential decay with effects localized near drivers and discontinuities, e.g. near boundary layers. The accuracy improvement for intermediate to high frequencies plays an important role in modeling control–structure interactions, dynamic localizations, acoustic fluid–structure interaction, scattering from inhomogeneities, and other applications requiring precise modeling of dynamic characteristics.

The numerical solution of the Reissner–Mindlin plate model for static analysis has been discussed by many authors. The primary focus has been various remedies to the well-known shear locking problem for very thin plates. Of the low order elements, the popular bilinear MITC4 ele-

ment [1] based on mixed interpolation of shear strains is one of the most attractive. The error analysis [2,3] performed on this element showed that it is optimally convergent for deflections and rotations on regular meshes. However, for the 4-node quadrilateral MITC4 element, it is not clear what is the optimal definition of the loading and mass which is consistent with the assumed strain field for dynamic analysis. While eliminating shear locking problems for thin plates, what is often overlooked is the large dispersion error exhibited in these elements leading to inaccurate resolution of propagating and evanescent wave behavior in dynamic analysis at intermediate to high frequencies. To address this problem, a residual-based modification of assumed strain mixed methods for Reissner–Mindlin plates is proposed. New plate elements are developed based on a generalized least-squares modification to the total energy for the time-harmonic Reissner–Mindlin plate model. Any of several existing mixed finite element interpolation fields which yield plate elements which are free from shear locking and pass the static patch test may be used. Here we start from the firm mathematical foundation inherent in the shear projection technique of the MITC4 element. A similar generalized least-squares approach was used in [4,5] to improved the accuracy of quadrilateral plate elements based

* Corresponding author. Tel.: +1 (864) 656-5631; Fax: +1 (864) 656-4435; E-mail: lonny.thompson@ces.clemson.edu

on assumed stress fields in a modified Hellinger–Reissner variational principle.

2. Wavenumber-frequency dispersion relation for Reissner–Mindlin plates

We consider the Reissner–Mindlin plate bending model with thickness t. The deformation is defined by

$$\boldsymbol{u} = -z\,\boldsymbol{\theta}(x, y) + w(x, y)\boldsymbol{e}_z, \tag{1}$$

where $\boldsymbol{\theta} = [\theta_x, \theta_y]^{\mathrm{T}} \in [H_0^1(A)]^2$ denotes the two-dimensional vector of rotations, such that $\boldsymbol{\theta} \perp \boldsymbol{e}_z$, and $w \in H_0^1(A)$ is the vertical deflection of the midsurface. The curvatures $\boldsymbol{\kappa}$, are defined through the symmetric part of the rotation gradient, $\boldsymbol{\kappa}(\boldsymbol{\theta}) := \nabla_s \boldsymbol{\theta}$. The transverse shear strains are defined by the angle between the slope of the midsurface after deformation and the section angle, $\boldsymbol{\gamma} = \nabla w - \boldsymbol{\theta}$. The inclusion of nonzero shear deformation in the Reissner–Mindlin model allows for a more accurate representation of high-frequency behavior.

In the following, we assume time-harmonic motion with assumed time-dependence $\mathrm{e}^{-\mathrm{i}\omega t}$, where ω is the circular frequency measured in rad/s. In the absence of an applied load q, the plate equations of motion admit solutions of the form

$$w = w_0\,\mathrm{e}^{(\mathrm{i}k\boldsymbol{\nu}\cdot\boldsymbol{x})}, \quad \boldsymbol{\theta} = \theta_0\boldsymbol{\nu}\,\mathrm{e}^{(\mathrm{i}k\boldsymbol{\nu}\cdot\boldsymbol{x})}, \quad \mathrm{div}\,\boldsymbol{\theta} = ik\theta_0\,\mathrm{e}^{(\mathrm{i}k\boldsymbol{\nu}\cdot\boldsymbol{x})}. \tag{2}$$

In the above, k is the wave number, $\boldsymbol{\nu} = [\cos\varphi, \sin\varphi]$ defines a unit vector in the direction of wave propagation, with wave vector $\boldsymbol{k} = k\boldsymbol{\nu} = k[\cos\varphi, \sin\varphi]$. Conditions for the allowed waves are obtained by substituting the assumed exponentials (2) into the homogeneous equations of motion. The result is the dispersion equation relating frequency ω to wave number k,

$$\mathcal{D}(k) := k^4 - (k_s^2 + k_p^2)k^2 + (k_p^2k_s^2 - k_b^4) = 0. \tag{3}$$

Here, $k_p = \omega/c_p$, $k_s = \omega/c_s$, $k_b = (\rho t\omega^2/D_b)^{1/4}$, where k_b is the classical plate bending wave number for in vacuo flexural waves in the Kirchoff theory, and

$$c_p = \left[\frac{E}{\rho(1-\nu^2)}\right]^{1/2}, \quad c_s = \left(\frac{G_s}{\rho}\right)^{1/2}. \tag{4}$$

In the above, $D_b = EI/(1-\nu^2)$, $I = t^3/12$, with Young's modulus E, Poisson's ratio ν, shear modulus G, and κ is a shear correction factor, $G_s = \kappa G$, and ρt is the mass density per unit area. Wave number solutions to the plate dispersion relation (3) occur in pairs: $\pm k_1$ and $\pm k_2$. At frequencies below a cut-off frequency, the wave number pair $\pm k_1$ occurs as purely real, while the pair $\pm k_2$ is purely imaginary. The real wave number pair corresponds to propagating waves while the imaginary pair corresponds to evanescent waves characterized by exponential decay.

3. Mixed least squares finite element formulation

To develop a residual-based mixed formulation, we start with the total energy functional for Reissner–Mindlin plates and then add weighted differential operators acting on the governing steady-state equations of motion written in least-squares form. This approach may be considered an extension of Galerkin Least Squares (GLS) methods to mixed or assumed strain methods. Recall the discrete total energy for the Mindlin plate model:

$$F_{\mathrm{M}}(\boldsymbol{\theta}^h, w^h) := \Pi_{\mathrm{M}}$$
$$+ \omega^2\frac{1}{2}\int_A [\rho t(w^h)^2 + \rho I(\boldsymbol{\theta}^h)^2]\,\mathrm{d}A - \int_A w^h q\,\mathrm{d}A, \tag{5}$$

$$\Pi_{\mathrm{M}} = \frac{1}{2}\mathrm{B}(\boldsymbol{\theta}^h, \boldsymbol{\theta}^h) + \frac{G_s t}{2}\int_A (\boldsymbol{\gamma}^h)^2\,\mathrm{d}A \tag{6}$$

$$\mathrm{B}(\boldsymbol{\theta}^h, \boldsymbol{\theta}^h) := \frac{EI}{(1+\nu)}$$
$$\times \left\{\int_A \boldsymbol{\kappa}(\boldsymbol{\theta}^h) : \boldsymbol{\kappa}(\boldsymbol{\theta}^h) + \left(\frac{\nu}{1-\nu}\right)(\mathrm{div}\,\boldsymbol{\theta}^h)^2\,\mathrm{d}A\right\}, \tag{7}$$

where $\boldsymbol{\gamma}^h$ is the assumed strain. Our Mixed Least Squares (MLS) method is then based on the functional:

$$F_{\mathrm{MLS}}(\boldsymbol{\theta}^h, w^h) = F_{\mathrm{M}} + F_{\mathrm{LS}}, \tag{8}$$

where

$$F_{\mathrm{LS}} = \sum_{A_e \in \mathcal{M}_h} \left\{\frac{1}{2}\int_{A_e} \tau_1(\nabla R_1^h)^2\,\mathrm{d}A + \frac{1}{2}\int_{A_e} \tau_2(R_2^h)^2\,\mathrm{d}A\right\} \tag{9}$$

is the least-squares modification. In the above,

$$R_1^h := D_s\,\mathrm{div}\,\boldsymbol{\gamma}^h + (\rho t\omega^2)w^h + q \tag{10}$$

$$R_2^h := (D_b\nabla^2 + \rho I\omega^2)\,\mathrm{div}\,\boldsymbol{\theta}^h + D_s\,\mathrm{div}\,\boldsymbol{\gamma}^h \tag{11}$$

are residuals for the finite element approximation to the governing equations for Mindlin plates. Here, $D_s = G_s t$, $\nabla^2 = \mathrm{div}\,\nabla$, and $\tau_1(\omega)$ and $\tau_2(\omega)$ are frequency dependent local mesh parameters determined from dispersion analysis and designed to improve the accuracy of the finite element solution. Any of several existing mixed finite element approximation fields which produce elements which are free from shear locking and pass the static patch test may be used. In this paper, we use the field- and edge-consistent interpolations of the MITC4 plate bending element proposed by Bathe and Dvorkin [1]. The finite element interpolation of the element domain A_e, together with the displacement field w^h, and $\boldsymbol{\theta}^h$, follows the standard isoparametric procedure. The displacement and rotation interpolation are constructed using the standard bilinear functions:

$$w^h(\xi, \eta) = \sum_{i=1}^{4} N_i(\xi, \eta)w_i, \quad \boldsymbol{\theta}^h(\xi, \eta) = \sum_{i=1}^{4} N_i(\xi, \eta)\boldsymbol{\theta}_i. \tag{12}$$

We let $[\boldsymbol{J}]$ be the Jacobian transformation matrix of the mapping $\boldsymbol{x}\colon \hat{A} \to A_e$, i.e. $\hat{\nabla} = [\boldsymbol{J}]^{\mathrm{T}}\nabla$, where $[\boldsymbol{J}] := [\boldsymbol{x}_{,\xi}]$, $J = \det[\boldsymbol{J}]$, and $\hat{\nabla}$ stands for the gradient operator with respect to ξ and η. For the MITC4 mixed interpolation [2,3], the assumed strain is defined by a reduction operator $\boldsymbol{R}_h\colon [H^1(A_e)]^2 \to \boldsymbol{\Gamma}_h(A_e)$, which maps the shear strain interpolants to an auxiliary space $\boldsymbol{\Gamma}_h$, $\boldsymbol{\gamma}^h = \boldsymbol{R}_h(\nabla w^h - \boldsymbol{\theta}^h) = (\nabla w^h - \boldsymbol{R}_h \boldsymbol{\theta}^h) = \nabla w^h - [\boldsymbol{J}]^{-T}\boldsymbol{R}_{\hat{A}}[\boldsymbol{J}]^{\mathrm{T}}\boldsymbol{\theta}^h$. The reduction operator $\boldsymbol{R}_{\hat{A}}\colon [H^1(\hat{A})]^2 \to \boldsymbol{S}^h(\hat{A}) = \{\boldsymbol{\epsilon} \mid \epsilon_1 = a_1 + b_1\eta, \epsilon_2 = a_2 + b_2\xi, a_1, b_1, a_2, b_2 \in \mathbb{R}\}$, is used to simplify the residuals appearing in the MLS functional.

For square element geometries, the divergence of the MITC4 interpolated shear strains vanishes within the element

$$\operatorname{div}\boldsymbol{\gamma}^h = \frac{1}{J}\hat{\nabla}\cdot\hat{\boldsymbol{\gamma}}^h = \frac{1}{J}(\gamma_{\xi,\xi} + \gamma_{\eta,\eta}) = 0. \qquad (13)$$

Furthermore, since $\boldsymbol{\theta}^h \in Q^1(\hat{A})$, then $\operatorname{div}\boldsymbol{\theta}^h \in P^1(\hat{A}) = \{\phi \mid \phi = c_1 + c_2\xi + c_3\eta, c_i \in \mathbb{R}\}$. With this result, it is clear that the Laplacian operator acting on the divergence of the rotations also vanishes for 4-node square elements, i.e.

$$\nabla^2(\operatorname{div}\boldsymbol{\theta}^h) = \frac{1}{J}\hat{\nabla}^2\left(\frac{1}{\sqrt{J}}\hat{\nabla}\cdot\boldsymbol{\theta}^h\right) = 0. \qquad (14)$$

Using (13) and (14) in (9), the generalized least-squares functional F_{LS} reduces to

$$F_{\mathrm{LS}} = \sum_{A_e \in \mathcal{M}_h} \frac{1}{2}\int_{A_e} r_1\nabla(w^h + f)\cdot\nabla(w^h + f)\,\mathrm{d}A$$
$$+ \frac{1}{2}\int_{A_e} r_2(\nabla\cdot\boldsymbol{\theta}^h)^2\,\mathrm{d}A, \qquad (15)$$

where $r_1 = \tau_1(\rho t\omega^2)^2$, $r_2 = \tau_2(\rho I\omega^2)^2$, and $f = q/(\rho t\omega^2)$.

Substituting the bilinear interpolations for w^h and $\boldsymbol{\theta}^h$, together with the assumed strain $\boldsymbol{\gamma}^h$ defined by the MITC4 interpolation, into Eq. (15) and imposing stationary conditions with respect to w^h and $\boldsymbol{\theta}^h$, results in the following system of linear algebraic equations for each element A_e,

$$[\boldsymbol{S}^e]\,\boldsymbol{d}^e = \boldsymbol{f}^e, \qquad (16)$$

where $\boldsymbol{d}^e$ is the 12×1 vector of element nodal displacements $\{(w_i, \boldsymbol{\theta}_i), i = 1, \ldots, 4\}$, $\boldsymbol{f}^e$ is the force vector resulting from the transverse loading, and $\boldsymbol{S}^e$ is the 12×12 symmetric dynamic stiffness matrix for each element,

$$\boldsymbol{S}^e(\omega) = \boldsymbol{Z}^e(\omega) + \boldsymbol{K}_{\mathrm{LS}}^e(\omega), \qquad (17)$$

where

$$\boldsymbol{Z}^e(\omega) = \boldsymbol{K}^e - \omega^2\boldsymbol{M}^e. \qquad (18)$$

Here, $\boldsymbol{K}^e$ and $\boldsymbol{M}^e$ are the stiffness and matrices for the plate, and $\boldsymbol{K}_{\mathrm{LS}}^e(\omega)$ is a stabilization matrix resulting from F_{LS}:

$$\boldsymbol{K}_{\mathrm{LS}}^e(\omega) = r_1(\omega)\boldsymbol{K}_{\mathrm{LS}1}^e + r_2(\omega)\boldsymbol{K}_{\mathrm{LS}2}^e \qquad (19)$$

with frequency independent matrices,

$$\boldsymbol{K}_{\mathrm{LS}1}^e = \int_{A_e}\{\boldsymbol{N}_{w,x}^{\mathrm{T}}\boldsymbol{N}_{w,x} + \boldsymbol{N}_{w,y}^{\mathrm{T}}\boldsymbol{N}_{w,y}\}\,\mathrm{d}A \qquad (20)$$

$$\boldsymbol{K}_{\mathrm{LS}2}^e = \int_{A_e}(\boldsymbol{N}_{\theta_x,x} + \boldsymbol{N}_{\theta_y,y})^{\mathrm{T}}(\boldsymbol{N}_{\theta_x,x} + \boldsymbol{N}_{\theta_y,y})\,\mathrm{d}A, \qquad (21)$$

where $\boldsymbol{N}_w$, $\boldsymbol{N}_{\theta_x}$ and $\boldsymbol{N}_{\theta_y}$ are row vectors of bilinear basis functions defined by the interpolations (12) written in vector form.

4. Evaluating element mesh parameters

Finite element difference relations associated with a typical node location (x_m, y_n) in a uniform mesh are obtained by assembling a patch of four elements. The result is a coupled system of three, 27-term difference stencils associated with the 3 nodal degrees-of-freedom at node (m, n). The effect of this stencil on the discrete solution $\boldsymbol{d}_{m,n}$ is written in matrix-vector form as

$$\sum_{p=-1}^{1}\sum_{q=-1}^{1}[\boldsymbol{D}_{pq}]\,E_x^p E_y^p\{\boldsymbol{d}\}_{m,n} = \{\boldsymbol{0}\}, \qquad (22)$$

where E_x^p and E_y^q are directional shift operators.

To obtain the finite element dispersion relation associated with this stencil, a plane wave solution is assumed for the nodal displacements, similar in form to the analytical solution:

$$\boldsymbol{d}_{m,n} = \begin{Bmatrix} w_0 \\ \theta_0\cos\varphi \\ \theta_0\sin\varphi \end{Bmatrix} \mathrm{e}^{(\mathrm{i}k_x^h hm)}\,\mathrm{e}^{(\mathrm{i}k_y^h hn)}, \qquad (23)$$

where $k_x^h = k^h\cos\varphi$, $k_y^h = k^h\sin\varphi$ are components of the wave vector $\boldsymbol{k}^h = k^h\boldsymbol{v}$, and h is the element length. Substitution of (23) into the stencil equations (22) results in the conditions for allowed waves in the finite element mesh: The resulting finite element dispersion relation for the plate is,

$$D := H_{11}H_{22} - H_{12}^2 = 0, \qquad (24)$$

where H_{ij} are functions of matrix coefficients z_{ij} of the element dynamic stiffness matrix $[\boldsymbol{Z}^e]$ defined in (18), wave angle φ, and r_1, r_2. The finite element dispersion equation $D = D(\omega, k^h h, \varphi, k_{ij}, m_{ij}, r_1, r_2)$ defined in (24) relates frequency ω, to the numerical wave number $k^h h$ and φ, and depends on the stiffness and mass coefficients $k_{ij} = [\boldsymbol{K}^e]_{ij}$, and $m_{ij} = [\boldsymbol{M}^e]_{ij}$, and mesh parameters r_1, r_2. Similar to the analytic dispersion relation, there are two pairs of numeric wave numbers $\pm k_1^h$ and $\pm k_2^h$ that satisfy (24) which correspond to propagating and evanescent waves, respectively.
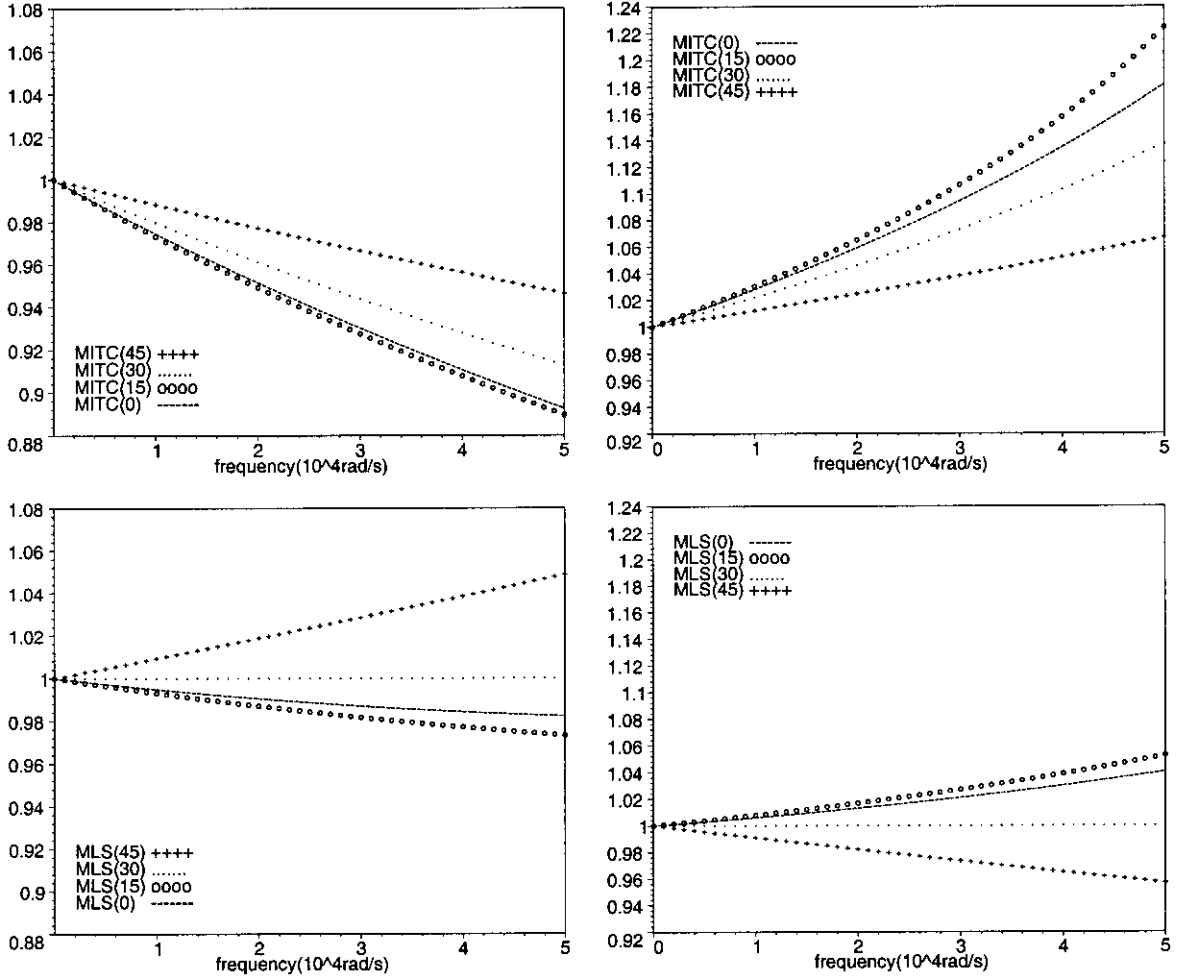
Fig. 1. Relative error k^h/k at angles $\varphi = 0, 15, 30, 45$ degrees. Top: MITC4. Bottom: MLS4 with $\varphi = 30°$ in definition of mesh parameters r_1 and r_2. Left: real propagating wave number k_1. Right: imaginary evanescent wave number k_2.

We determine design parameters r_1 and r_2 such that the finite element wave number pairs match the analytical wave number pairs $\pm k_1$ and $\pm k_2$ for a given orientation $\varphi = \varphi_0$. Here, optimal values for r_1 and r_2 are computed by setting $k^h = k_1(\omega)$ and $k^h = k_2(\omega)$ in the finite element dispersion relation (24). The result is two equations which may be solved for the mesh parameters $r_1(\varphi, \omega, h)$ and $r_2(\varphi, \omega, h)$:

$$c_{11} + c_{12}r_1 + c_{13}r_2 + c_{14}r_1r_2 = 0 \tag{25}$$

$$c_{21} + c_{22}r_1 + c_{23}r_2 + c_{24}r_1r_2 = 0 \tag{26}$$

with coefficients $c_{1i} = c_i(k_1, \varphi)$, and $c_{2i} = c_i(k_2, \varphi)$.

Eliminating r_2 from (25) and (26), allows the design parameter r_1 to be obtained in closed-form by solving the quadratic equation,

$$e_1r_1^2 + e_2r_1 + e_3 = 0, \tag{27}$$

where $e_l = e_l(c_{ij})$. The solution of (27) results in two real negative roots. We select the largest root to determine r_1,

as this root matches the analytical dispersion relations. The other design parameter can then be written in terms of the first,

$$r_2 = -\frac{c_{21}r_1 + c_{11}}{c_{31} + c_{41}r_1}. \tag{28}$$

Hence, the design parameters $r_l = r_l(k_{ij}, m_{ij}, \omega, h, \varphi)$, $l = 1, 2$ are obtained in terms of the stiffness and mass coefficients in the underlying MITC4 element, the frequency dependent wave numbers satisfying the analytical dispersion relation, and φ. Using our definitions for r_1 and r_2, for a fixed angle φ, the least-squares modification enables the finite element wave numbers to exactly match the analytical dispersion conditions, rendering a zero dispersion error solution. In general, the direction of wave propagation φ is not known a priori. However, similar to [6], we can select a φ in the definitions for r_1 and r_2 which minimizes dispersion error over the entire range of possible angles defined by the periodic interval $0 \leq \varphi \leq \pi/4$.

In implementing our mixed least squares method on nonuniform meshes, the element length h is defined by either a local size determined by the square root of the element area, $h_e = \sqrt{A_e}$, or by an average element length h_{ave} computed over a local patch of similarly sized elements. While the optimal definition for the mesh parameters r_1 and r_2 were derived from a dispersion relation on a uniform mesh, with constant element length h, accurate solutions on nonuniform meshes are shown to be relatively insensitive to the precise definitions used for h.

5. Dispersion accuracy

For a range of frequencies ω, and wave angles φ, relative to uniform mesh lines, the wave number accuracy for our residual-based MLS method is compared with the underlying MITC method [1]. Results are presented for a steel plate with properties: $E = 210 \times 10^{10}$ dynes/cm^2, $\nu = 0.29$, $\rho = 7.8$ g/cm^2, plate thickness $t = 0.15$ cm, and shear correction factor $\kappa = 5/6$.

The relative error of the numerical wave number divided by the analytic wave number, k^h/k is shown in Fig. 1. The frequency range is plotted over the range up to $\omega h = 5 \times 10^4$ cm/s corresponding to approximately four elements per wavelength. At low frequencies, the MITC4 element replicates the character of the analytic dispersion curves marginally well with error in the real propagating wave number less than 3% for discretizations finer than 10 elements per wavelength, i.e. $10h = \lambda$. However, above this level, the error in both the real and imaginary wave number increases rapidly. To achieve a 1.5% level of accuracy would require more than 20 MITC4 plate elements per wavelength.

The bottom two plots show the improved dispersion accuracy achieved for both the real and imaginary wave numbers by our residual-based MLS4 element. The MLS4 element replicates the character of the analytical dispersion curves well with significant reduction in numerical wave number error compared to the underlying MITC4 interpolation. Results for the MLS4 method give a maximum error in the real wave number less than 1% at a frequency of $\omega h = 1 \times 10^4$ cm/s, corresponding to approximately 10 el-

ements per wavelength. This represents a nearly three-fold reduction in phase accuracy compared to the base MITC4 element. At the level of 10 elements per wavelength, the maximum error in the imaginary wave number is reduced from 3% for MITC4 to less than 2% for MLS4.

6. Numerical example

Results are presented for forced vibration of a simply supported steel plate with a uniform distributed time-harmonic pressure loading $q = 2$ dynes/cm^2. Fig. 2 shows the L_2 convergence rates for the vertical deflection with uniform mesh refinement. Both MITC4 and MLS4 achieve the same rate of convergence at approximately $N = 100$ elements. However, as a result of improved dispersion accuracy, the MLS4 element decreases the L_2 error for the same number of elements.

We next study the performance of the MLS4 element for quasi-uniform meshes (parametric mesh grading). Here, the MLS4 element is computed with mesh parameters r_1 and r_2 determined from an average element size h_{ave},
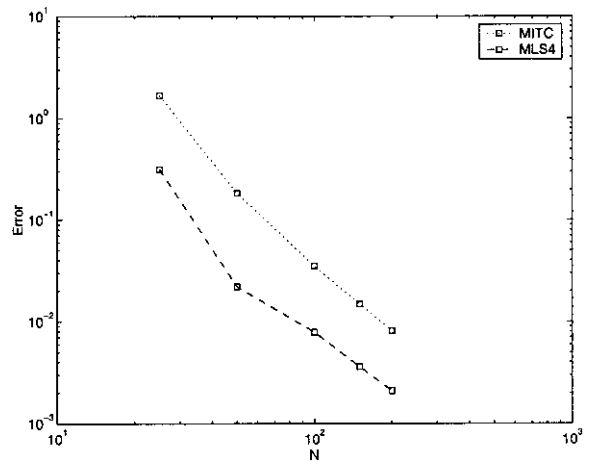
Fig. 2. Simply supported steel plate example. Frequency $f = 500$ Hz. Convergence with mesh refinement. Relative discrete L_2 error of vertical deflection versus N, for a uniform mesh of $N \times N$ elements over one-quarter of the plate.

Table 1
Discrete L_2 error for square plate example with quasi-uniform meshes at $f = 500$ Hz

Mesh	Element type			
	SRI4	MITC4	MLS4-ave	MLS4-local
QMesh1	0.29952E 0	0.29952E 0	0.55688E$-$1	0.38146E$-$1
QMesh2	0.38511E 0	0.38514E 0	0.12876E 0	0.52325E$-$1
QMesh3	0.33728E 0	0.33731E 0	0.32663E$-$1	0.33728E$-$1
Uniform	0.18351E 0	0.18352E 0	0.22147E$-$1	0.22147E$-$1

Results for a uniform mesh with equally spaced nodes shown for reference.
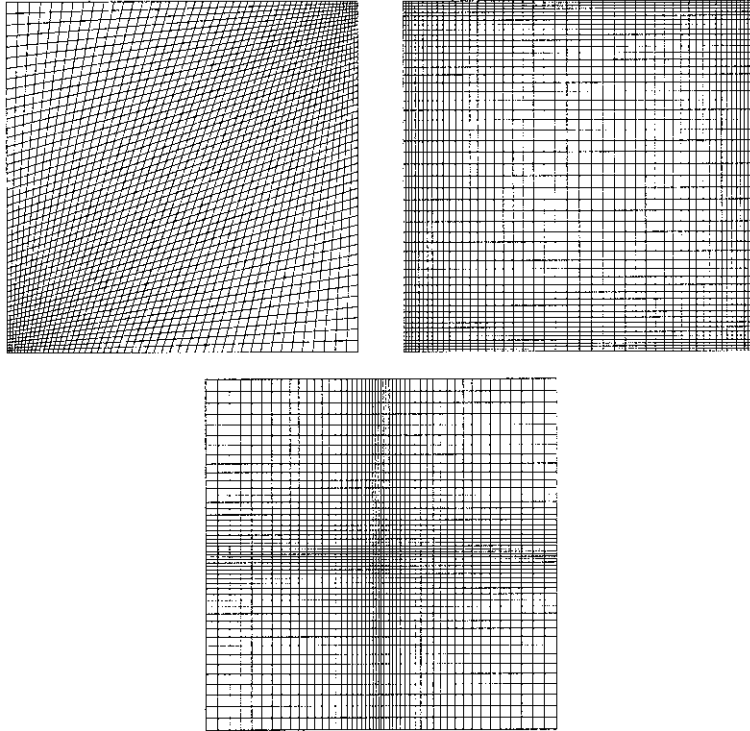
Fig. 3. Quasi-uniform meshes with $N = 50$ elements per edge and $5:1$ bias. Average element size $h_{\mathrm{ave}} = \sqrt{A/N_T} = 1.0$. (Left) QMesh1, (Right) QMesh2, (Bottom) QMesh3.

computed over the total mesh, denoted MLS4-ave, and from a local element size $h_e = \sqrt{A_e}$, denoted MLS4-local. Table 1 shows results obtained using the three different quasi-uniform meshes shown in Fig. 3. We observe that the large improvement in accuracy using the MLS4 element compared to the MITC4 element for uniform meshes is not drastically affected by the element distortions or higher aspect ratios. Showing the robustness of the MLS method, the discrete L_2 error for the MLS4-local solution remains an order of magnitude lower than the underlying MITC4 element.

7. Conclusions

A residual-based method for improving the dispersion accuracy of the 4-node MITC plate bending elements is developed. The property of field consistency in the MITC transverse shear strain interpolation is used to simplify the residuals appearing in the generalized least-squares operators, and leads to a simple modification of the element dynamic stiffness matrix with a frequency-dependent least-squares matrix. Using complex wave number dispersion analysis, optimal values for the mesh parameters appearing in the least-squares matrix are determined such that finite element propagating and evanescent wave number pairs

match the analytical wave number pairs for a given wave orientation angle φ relative to a uniform mesh. Both dispersion analysis and numerical results show that the new mixed least-squares (MLS4) plate element significantly improves wave accuracy compared to the underlying MITC4 element.

Acknowledgements

References

[1] Bathe KJ, Dvorkin E. A four node plate bending element based on Mindlin–Reissner plate theory and mixed interpolation. Int J Num Methods Eng 1985;21:367–383.

[2] Bathe KJ, Brezzi F. On the convergence of a four-node plate bending element based on Mindlin/Reissner plate theory and mixed interpolation. In: Whiteman JR (Ed.), Proc Conf Math Finite Elements Appl V, Academic Press, New York, 1985, pp. 491–503.

[3] Bathe KJ, Brezzi F. A simplified analysis of two plate bending elements — the MITC4 and MITC9 elements. In: GN Pande, J Middleton (Eds.), Proc Int Conf Num Methods Eng, (NUMETA 87), Martinus Nijhoff, Dordrecht, 1987.

[4] Thompson LL, Tong Y. Hybrid Least Squares Finite Element Methods for Reissner–Mindlin Plates. Comput Methods Appl Mech Eng, accepted for publication.

[5] Thompson LL, Tong Y. Hybrid least squares finite element methods for Reissner–Mindlin plates. In: Proceedings of the ASME Noise Control and Acoustics Division – 1999, 1999 ASME International Mechanical Engineering Congress and Exposition, ASME, NCA Vol. 26, 1999, pp. 77–89.

[6] Thompson LL, Pinsky PM. A Galerkin least squares finite element method for the two-dimensional Helmholtz equation. Int J Num Methods Eng 1995;38:371–397.